ANNALS OF GEOPHYSICS, 68, 6, S686, 2025; doi:10.4401/ag-9340
OPEN ACCESS

Inversion of Rayleigh wave dispersion data based on variational modal decomposition football team training algorithm

Ma Zhenwei[1,2], Yao Zhenan[*,1], Li Hongxing[1,2], Xie Yun[1,2], Zeng Haoyu[1,2]

(1) Jiangxi Provincial Earthquake Disaster Mitigation and Engineering Geological Disaster Detection Engineering Research Center, East China University of Technology, Nanchang, Jiangxi
(2) State Key Laboratory of Nuclear Resources and Environment, East China University of Technology, Nanchang, Jiangxi

Article history: received March 25, 2025; accepted October 10, 2025

Abstract

In view of the triple challenges in the Rayleigh wave dispersion curve inversion algorithm, which has strong sensitivity, low convergence efficiency and poor noise robustness, The Football Team Training Algorithm (FTTA) is applied to the problem of dispersion curve inversion,; and proposes a Variational Football Team Training Algorithm, VFTTA)'s Rayleigh wave dispersion curve inversion method, which introduces variational modal decomposition (VMD) into the FTTA to build a hybrid inversion framework. The core innovation lies in: i) Constructing a three-stage mapping mechanism for football training – to achieve efficient parameter space search through global collaborative collective training, regional optimization group training, and individual reinforcement additional training; ii) Design a VMD-FTTA joint preprocessing system, FTTA is used to adaptively optimize VMD parameters to achieve optimal decomposition of the original signal and accurate extraction of the target mode, fundamentally suppressing noise interference and providing high-fidelity input signals for inversion. This study first tested the performance of FTTA and VFTTA through two complex benchmark functions and then applied it to the inversion of noise-containing and noise-free base-order and higher-order dispersion curves designed under different geological conditions. The results show the effectiveness and reliability of VFTTA in dispersion curve inversion. Finally, the measured micro-motion dispersion data in Nanjing area further verified that VFTTA has smaller fitting errors and higher stability compared with FTTA and PSO.

Keywords: Rayleigh Surface Wave; Dispersion Curve Inversion; Global Optimization Algorithm; Football Team Training Algorithm; VMD-FTTA Joint Preprocessing System

1. Introduction

Since the discovery of Rayleigh waves in 1887, this type of seismic wave, once considered as noise, has developed into a core technology for shallow exploration. Its physical essence originates from the coupling of P waves and SV waves at the free interface. When the velocity and thickness of the formation change, the dispersion phenomenon (phase

velocity changes with frequency) generated by Rayleigh waves provides a key information chain for the inversion of underground medium parameters. Dispersion curve inversion is a key link in Rayleigh wave exploration, and its results directly affect the interpretation and reliability of formation information.

At present, there are two core calculation methods in the field of dispersion curve inversion: local linear optimization algorithm and global nonlinear optimization algorithm. In view of the multi-solution and uncertainty problems of inversion caused by the nonlinear characteristics of underground media, local linear optimization algorithms show unique application value. The core mechanism of this type of method is to transform nonlinear mathematical models into linear systems for solution. Its representative algorithms include least squares method, singular value decomposition algorithm and Occam inversion algorithm. At the specific application level, although the least squares method can effectively obtain shear wave velocity and formation thickness parameters, its calculation results are closely related to the setting of the initial model. The singular value decomposition algorithm and the Occam algorithm can realize automated stratigraphic division and parameter inversion with the advantages of higher numerical stability and computational accuracy. It is worth noting that this type of traditional algorithm still has inherent defects such as high initial model sensitivity, complex parameter system, and easy to fall into local optimal solution. At the same time, it is necessary to construct a partial derivative matrix to determine the gradient direction. These technical bottlenecks restrict their application effect in complex scenarios. In comparison, the global nonlinear optimization algorithm performs outstandingly in reducing the dependence on the initial model and enhancing the global search capability and is particularly suitable for solving strong nonlinear inversion problems. This algorithm group includes genetic algorithms, simulated annealing algorithms, particle swarm optimization algorithms, etc., which simulate the natural evolution law or group intelligent behavior to traverse the parameter space, effectively avoiding the local extreme value trap while improving the probability of obtaining the global optimal solution. This optimization mechanism based on the principle of bionics enables the global nonlinear method to show more significant technical advantages and application potential in the field of surface wave dispersion curve inversion.

However, algorithms such as the classic genetic algorithm (GA), simulated annealing (SA), and particle swarm optimization (PSO) have weak ability to jump out of local optimality, are highly dependent on parameter selection, and have problems of instability and slow convergence in the inversion of noisy data. However, the measured data often contain a lot of noise, such as lightning, radio waves, traffic noise, etc., which will interfere with the observation data. In order to eliminate noise interference and improve the signal-to-noise ratio of the data, in 2016, Li Huailiang et al. added a finite difference algorithm to the multi-wave acquisition technology to eliminate the boundary influence of the undulating surface and effectively suppress the interference wave. Although the corresponding denoising method has been adopted, the noise in the data cannot be completely eliminated. Therefore, in the inversion of the dispersion curve of noisy data, it is necessary to select an algorithm with better noise resistance to improve this problem.

As an emerging swarm intelligence optimization method, FTTA has shown significant advantages in path planning and complex optimization problems in recent years. For example, Li et al. (2024) verified the efficient convergence of FTTA in UAV path planning; Peng et al. (2024) improved the algorithm's ability to escape from local optimality by embedding Tent chaotic mapping; and the dual fitness function framework designed by Hou et al. (2024) effectively solved the Pareto frontier equilibrium problem in multi-objective optimization. It is particularly noteworthy that the dynamic environment perception mechanism proposed by Wang (2025) further expanded the application potential of FTTA in real-time scenarios, and its adaptive step size strategy improved the convergence efficiency of the algorithm in dynamic path planning by more than 30%.

In the field of Rayleigh wave dispersion curve inversion, the innovative application of swarm intelligence algorithms has become a research hotspot in recent years. The adaptive logarithmic spiral-Lévy firefly algorithm proposed by Liu et al. (2023) significantly improved the inversion accuracy and global search capability by integrating the spiral search path and the Lévy flight mechanism. Its anti-noise performance is particularly suitable for dispersion curve inversion under complex geological conditions. The sine-cosine algorithm of Fu et al. (2023) effectively suppresses premature convergence by using periodic oscillation characteristics and performs well in the inversion of low-speed interlayer models. In addition, the Osprey-Cauchy-Dove optimization algorithm developed by Liu et al. (2025) balances exploration and development capabilities through a three-stage search framework and reduces the error rate by 15% compared with traditional methods in the inversion of geological models containing high-speed hard interlayers.

VFTTA is applied to dispersion curve inversion. The VFTTA algorithm is inspired by the behavior of players in high-level football training classes. By simulating three stages of collective training, group training and

individual additional training, the global search ability and local search accuracy of the algorithm are improved. In the collective training stage, the players are divided into four types: followers, discoverers, thinkers and undulators. Different search strategies are simulated by randomly changing the types. In the group training stage, the players are divided into different roles according to their characteristics and receive targeted training. In the individual additional training stage, personalized training is carried out to improve skills. The VFTTA algorithm can be directly applied to optimization problems without complex parameter adjustment. This study first verified the optimization performance of FTTA compared with other algorithms through the test of two complex benchmark functions. In the dispersion curve inversion, the data preprocessing strategy combining variational mode decomposition (VMD) and football team training algorithm (FTTA) can effectively extract Rayleigh wave phase velocity information from seismic data. First, VMD decomposes the complex seismic signal into a series of intrinsic mode functions (IMFS) and then optimizes the penalty factor α and the number of decomposition layers k of VMD through FTTA to minimize the envelope entropy, identify and remove the noise component. This process not only improves the quality of signal decomposition but also enhances the accuracy of subsequent formation parameter inversion, making the Rayleigh wave phase velocity calculated from the optimized denoised signal more reliable, thereby providing more accurate formation physical parameters for seismic exploration and related engineering applications. Subsequently, FTTA, VFTTA and PSO were applied to the inversion of noisy and noise-free fundamental and high-order dispersion curves. The results show that VFTTA performs best in dispersion curve inversion, with smaller fitting error, higher logging data matching and stronger stability. Through the inversion experiment of measured micro-motion dispersion data in Hangzhou area, the significant advantages of VFTTA compared with PSO and FTTA in the inversion of surface wave dispersion data were verified, and it also provides a theoretical basis and practical reference for its application in other geophysical inversion problems.

2. Basic principles of FTTA

In this section, the mathematical model of FTTA is given, including the initialization phase, collective training phase, group training phase, and individual additional training phase. In FTTA, as in other swarm intelligence optimization algorithms, the initial value of each solution can be given based on prior information. If prior information is not available, the initial set can be randomly generated. Then the position update equations of these solutions are as follows:

$$X_i^1 = lb + rand \times (ub - lb), i = 1,2, \dots, N \tag{1}$$

where X_i^1 represents the i position of the current solution in the first dimension at the first iteration. ub and lb represent the upper and lower bounds of the search space, respectively. N is the number of FTTA populations. $rand$ represents a random number between 0 and 1.

The initial population can be represented as follows:

$$X = \begin{bmatrix} X_1 \\ X_2 \\ \vdots \\ X_i \\ \vdots \\ X_N \end{bmatrix} = \begin{bmatrix} X_{1,1} & X_{1,2} & \cdots & X_{1,j} & \cdots & X_{1,Dim} \\ X_{2,1} & X_{2,2} & \cdots & X_{2,j} & \cdots & X_{2,Dim} \\ \vdots & \vdots & \vdots & \vdots & \vdots & \vdots \\ X_{i,1} & X_{i,2} & \cdots & X_{i,j} & \cdots & X_{i,Dim} \\ \vdots & \vdots & \vdots & \vdots & \vdots & \vdots \\ X_{N,1} & X_{N,2} & \cdots & X_{N,j} & \cdots & X_{N,Dim} \end{bmatrix} \tag{2}$$

where $X_{i,j}$ represents the j position of the i solution and Dim represents the dimension size.

The Football Team Training Algorithm (FTTA) is implemented by simulating the behavior of players in high-level football training sessions. Usually, football training sessions are divided into three parts: collective training, small group training, and individual additional training. The specific behavior and equation are as follows:

2.1 Group training

At the beginning of the training, the players will conduct collective training under the guidance of the coach, who will first let the players know their level through a series of tests (physical functions). Then the players will make their own collective training plan according to their level. We divide the players into four different types: Followers, Finders, Thinkers and Fluctuators. In each iteration, the players will randomly change their type.

2.1.1 Followers

The follower is a fanatical follower of the current best player. He strives towards the best player in each dimension, hoping to reach the level of the current best player, but due to the limitation of power, he can only move randomly to the best player in each dimension. The equation is as follows:

$$F_{i,j}^{k}new = F_{i,j}^{k}old + rand \times \left(F_{best,j}^{k} - F_{i,j}^{k}old\right) \tag{3}$$

The current best player is defined as F_{best}^{k}, where k is the number of iterations and $F_{best,j}^{k}$ is its value on dimension j; the current player is defined as $F_{i,j}^{k}$; i is its number of players, $F_{i,j}^{k}$ is its value on dimension j, and $F_{i,j}^{k}new$ is the state of the player on dimension j after training.

2.1.2 Discoverer

Finders are more rational than followers. They not only see the best players, but also the worst players, so they not only work towards the best players, but also try their best to avoid becoming the worst players. The equation is as follows:

$$F_{i,j}^{k}new = F_{i,j}^{k}old + rand_1 \times \left(F_{best,j}^{k} - F_{i,j}^{k}old\right) - rand_2 \times \left(F_{worst,j}^{k} - F_{i,j}^{k}old\right) \tag{4}$$

where the current worst player is defined as F_{worst}^{k}, k is the iteration number, where $F_{worst,j}^{k}$ is its value in dimension j. $F_{i,j}^{k}new$ is the state of the player in dimension j after training.

2.1.3 Thinker

Thinkers are more alert than those before them, they see directly the gap between the best players and the worst players, and work hard to reach the gap in each dimension, the equation is as follows:

$$F_{i,j}^{k}new = F_{i,j}^{k}old + rand \times \left(F_{best,j}^{k} - F_{worst,j}^{k}\right) \tag{5}$$

In the dimension j, $F_{best,j}^{k} - F_{worst,j}^{k}$ is the difference vector between the current best player and the worst player, and k is the number of iterations.

2.1.4 Fluctuator

Volatility refuses to learn from anyone, they train themselves, so the state will have a certain fluctuation. Of course, as the number of training increases (number of iterations), the fluctuation of the player's state will become smaller and smaller. We define the change of the player's state as follows:

$$F_{i,j}^{k}new = F_{i,j}^{k}old \times \left(1 + t(k)\right) \tag{6}$$

where $t(k)$ is a random number with distribution t, and its degree of freedom is the current number of iterations. As the degree of freedom increases, the probability of the t distribution approaching the middle value (0) becomes higher and higher, and the distribution at both ends gradually decreases, and will become closer and closer to the normal distribution. Therefore, as the number of iterations increases, the degree of fluctuation will become smaller and smaller, and gradually change from global search to local search.

2.2 Group training

After the collective training, the football training process has entered the group training stage. The coach divides the players into four categories according to their characteristics (each dimension is a feature value): forward, midfielder, defender and goalkeeper. In the group training, the football team training algorithm (FTTA) adopts the MGEM adaptive clustering method (MixGaussEM) to simulate the coach's behavior through the clustering method and divide the crowd into four categories according to their own characteristics.

$$\begin{gathered} All\ Players \xrightarrow{MGEM} [Team1, Team2, Team3, Team4] \\ if\ Any\ team \leq Team\ number \\ All\ Players \xrightarrow{Randomuniformgrouping} [Team1, Team2, Team3, Team4] \end{gathered} \tag{7}$$

A threshold, termed team number ($Team\ number \geq 2$), is established as the minimum required number of individuals in each group. It is assumed that if the number of groups falls below this value, group training cannot be effectively implemented. In such cases, a secondary grouping process is initiated, where a uniform random grouping strategy is employed to randomly and evenly distribute the participants into four distinct groups.

After the coach completes the grouping, the players will learn or communicate with other players in the group. We define group training as three states: optimal learning, random learning, and random communication. We define the learning probability as $pstudy$, the communication probability as $pcomm$, and the player will randomly select the state in each iteration.

2.2.1 Optimal Learning

In each dimension, a player has a certain probability to directly learn the ability value of the best player in the group. The equation is defined as follows:

$$F_{i,j}^{k,team}new = \begin{Bmatrix} F_{best,j}^{k,team_l}, if\ rand \leq p_{study} \\ F_{i,j}^{k,team_l}old, if\ rand > p_{study} \end{Bmatrix} \tag{8}$$

where $F_{best}^{k,team_l}$ is the best player in the l group, k is the number of iterations, $team_l$ represents the l group, $F_{best,j}^{k,team_l}$ is the j dimension of the best player of the l group, and $F_{i,j}^{k,team_l}new$ is the state of the player in dimension j after optimal learning.

2.2.2 Stochastic Learning

In each dimension, the player has a certain probability to directly learn the ability value of any random player in the group. The equation is defined as follows:

$$F_{i,j}^{k,team_l}new = \begin{Bmatrix} F_{random,j}^{k,team_l}, if\ rand \leq p_{study} \\ F_{i,j}^{k,team_l}old, if\ rand > p_{study} \end{Bmatrix} \tag{9}$$

where $F_{random}^{k,team_l}$ is a random player in the l group, k is the number of iterations, $team_l$ represents the l group, $F_{random,j}^{k,team_l}$ is the j dimension of the random player of the l group, and $F_{i,j}^{k,team_l}new$ is the state of the player in the j dimension after random learning.

2.2.3 Random communication

In training, learning is only part of it, and communication between two players is more important for the improvement of ability. In each dimension, a player has a certain probability of communicating with any player in the group.

At that time $rand \leq pcomm$, the equation was defined as follows:

$$\begin{aligned} F_{i,j}^{k,team_l}new &= F_{random,j}^{k,team_l}old \times (1 + randn) \\ F_{random,j}^{k,team_l}new &= F_{i,j}^{k,team_l}old \times (1 + randn) \end{aligned} \tag{10}$$

where $F_{random}^{k,team_l}$ is a random player in the l group, k is the number of iterations, $team_l$ represents the l group, $F_{random,j}^{k,team_l}$ is the j dimension of the random player in the l group, and the two players exchanged their abilities in dimension. $randn$ is a normally distributed random number, multiplied by $(1 + randn)$ represents the two players' understanding of the others' abilities.

At that time $rand > pcomm$, the equation was defined as follows:

$$\begin{aligned} F_{i,j}^{k,team_l}new &= F_{i,j}^{k,team_l}old \\ F_{random,j}^{k,team_l}new &= F_{random,j}^{k,team_l}old \end{aligned} \tag{11}$$

2.2.4 Random Error

Assume that during group training, there is a certain probability that errors will occur, that is, they accidentally learn the content of other dimensions of others. The probability of this happening is low, but it is real and objective. We define the error probability as p_{error}.

$$\begin{aligned} F_{i,j}^{k,team_l}new &= F_{random1,random2}^{k,team_l}old, if\ rand \leq p_{error} \\ F_{i,j}^{k,team_l}new &= F_{i,j}^{k,team_l}old, if\ rand > p_{error} \end{aligned} \tag{12}$$

2.2.5 Additional personal training

After the group training is over, it is necessary to recalculate the new physical fitness value and replace the poor physical fitness value with the better physical fitness value to update the player's status. After the update, the coach will select the best player, let him practice, and make him better, so that he can better lead the training status of others. The training equation is as follows:

$$F_{best}^{k}new = F_{best}^{k}old \times \left(1 + (1 - 1/k)\right) \times Gauss + 1/k \times Cauchy \tag{13}$$

Cauchy and Gaussian joint mutation is used to describe individual additional training, which is the number of iterations. The reason why Gaussian Cauchy distribution is chosen is that in the early stages of training, everyone's level is usually not high, so the best players have a greater probability of getting a greater improvement. At this time, the Cauchy distribution function occupies a large proportion, which can effectively provide players

with a large range of improvements, which is conducive to global search. As the number of iterations increases, it becomes more and more difficult to improve the player's ability. At this time, the Gaussian distribution accounts for a large proportion, and the player's promotion range gradually decreases, which is more conducive to local search.

The above-mentioned Cauchy-Gaussian mixed mutation mechanism provides the algorithm with the ability to dynamically balance global exploration and local development, and how to effectively embed this optimization strategy into the seismic signal processing process requires the construction of a complete computational framework.

3. Improvement strategy

Since noise can significantly affect the extraction accuracy of dispersion curves, when the noisy surface wave signal is converted into a dispersion energy map, the extracted dispersion curve will have certain disturbances, resulting in errors, which in turn affect the accuracy of the inversion results. In order to solve this problem, this study established a VMD-FTTA joint optimization system, which uses FTTA to optimize the hyperparameters of VMD, achieves noise suppression of seismic data, and then uses the denoised data to achieve high-precision dispersion curve inversion under the FTTA inversion framework.

VMD is an adaptive and efficient signal decomposition method that can decompose non-stationary signals into different modal components according to the center frequency and bandwidth, thereby separating the effective signal and noise according to different modal components. The decomposition process of VMD is actually the construction and solution process of variational problems. Its constrained variational model is as follows:

$$\{u_k\}^{min},\{\omega_k\}\left\{\sum_{k=1}^{K}\left\|\partial_t\left\{\left[\left(\delta(t)+\frac{j}{\pi t}\right)*u_k(t)\right]e^{-j\omega_k t}\right\}\right\|_2^2\right\}\cdot s.t.\sum_{k=1}^{K}u_k=f \tag{14}$$

where u_k is the IMF component with band-limited properties after VMD decomposition; ω_k is the frequency center of the corresponding mode: $\delta(t)$ is the Dirac function; * is the convolution calculation symbol; f is the original real-valued signal. The meaning of $\left(\delta(t)+\frac{j}{\pi t}\right)*u_k(t)$ is to transform each modal function into an analytical signal through the Hilbert transform and transform the real-valued signal u_k into a complex-valued form to obtain the unilateral spectrum of u_k. When solving this problem, the constrained variational model can be transformed into an unconstrained variational model, and then the modal components and their center frequencies can be obtained in the iterative process of finding the optimal solution.

In the Lagrange multiplier method, α is used as the coefficient of the quadratic penalty term to balance the strictness of the constraint conditions (i.e. the approximation degree of the sum of the modal component IMFs to the original signal). The larger α is, the stricter the bandwidth constraint of the modal component is (each IMF is narrower), but the transient characteristics may be over-smoothed; the smaller α is, the wider the bandwidth is allowed, but modal aliasing may be introduced.

$$\mathrm{L}(\{u_k\},\{\omega_k\},\lambda)=\alpha\sum_{k=1}^{K}\partial_k\left[\left(\delta(t)+\frac{j}{\pi t}\right)*u_k(t)\right]e^{-j\omega_k t}\frac{2}{2}+f(t)-\sum_{k=1}^{K}u_k(t)_2^2+\langle\lambda(t),f(t)\rangle \tag{15}$$

In the objective function and constraints, k explicitly limits the total number of modal component IMFs. If k is too small, the signal will be under-decomposed (effective components will be lost), while if k is too large, false modes will be introduced (overfitting).

VFTTA is mainly based on variational mode decomposition (VMD) and FTTA and uses FTTA to optimize the penalty factor α and the number of decomposition layers k of VMD to achieve the best data preprocessing effect. The component with the largest fluctuation in the decomposed IMF components is deleted as white noise, and the other IMF components are reorganized to obtain the denoised time series data.

Objective function design: VFTTA is an advanced data preprocessing model. In this model, the fitness function of FTTA is the minimum value of envelope entropy, and envelope entropy represents the sparse characteristics of the original signal. When there is more noise and less feature information in the IMF, the envelope entropy is larger, otherwise, the envelope entropy is smaller.

In the signal $x(i)$, the envelope entropy E_p is calculated using the following equation:

$$E_p = -\sum_{j=1}^{N} p_j \lg p_j p_j = \frac{a(j)}{\sum_{j=1}^{N} a(j)} \tag{16}$$

where $a(j)$ is the envelope signal of k modal components decomposed by VMD and demodulated by Hilbert. p_j is the probability distribution sequence obtained by calculating the normalization of $a(j)$. N is the number of sampling points, and the entropy of the probability distribution sequence is the envelope entropy E_p. After VFTTA optimization, the optimal hyperparameters $[\alpha, k]$ are obtained, and the best data preprocessing effect is achieved.

The algorithm flow of VFTTA is shown in Fig. 1.

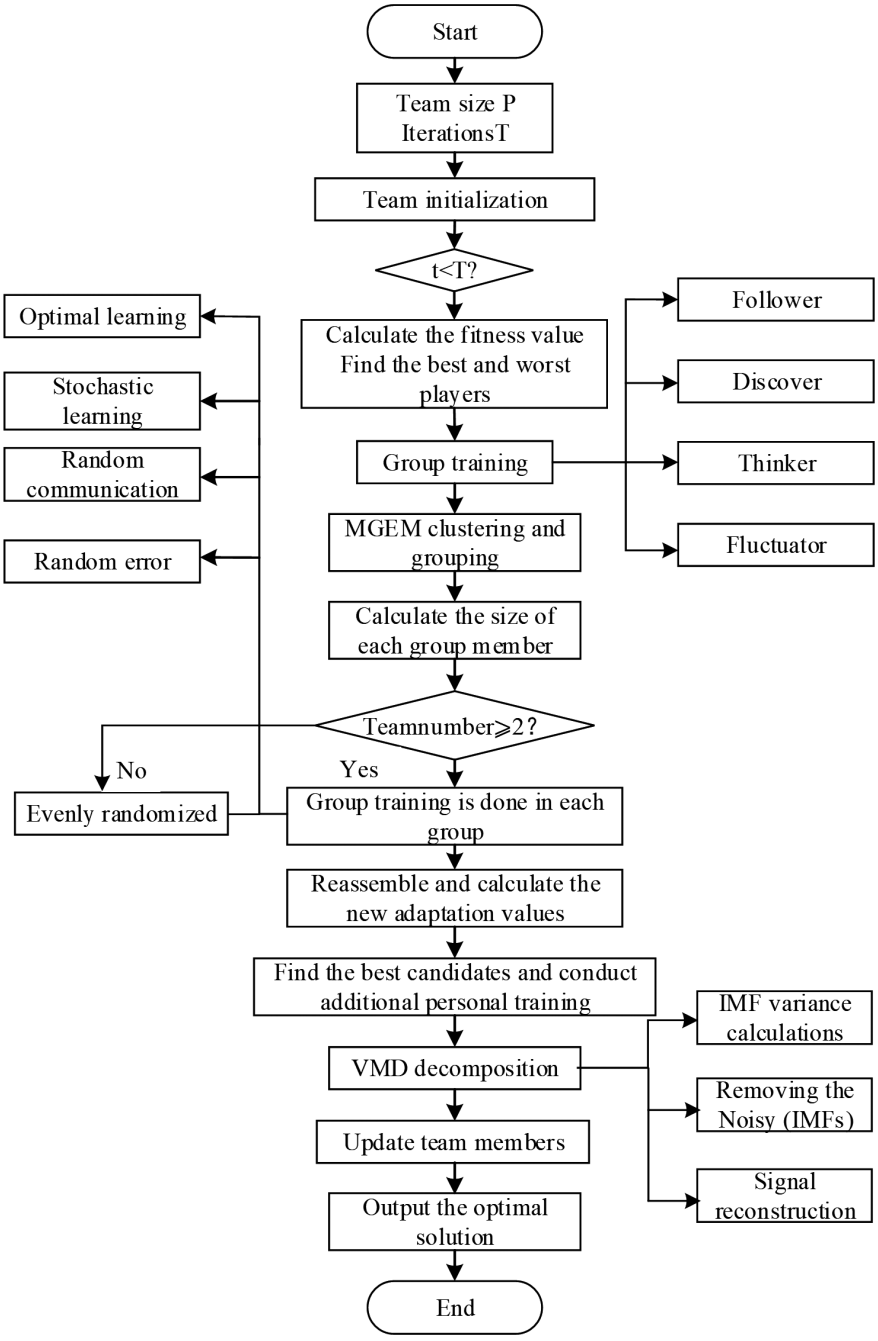

Figure 1. VFTTA flow chart.

4. Objective function test

4.1 Comparison of algorithms

To evaluate the performance of VFTTA, a comparative analysis is conducted against PSO and FTTA. PSO was proposed by Kennedy in 1995 to simulate the foraging behavior of bird flocks. It is an efficient meta-heuristic optimization method. Due to its fast convergence speed and simple parameter adjustment, PSO has been widely used in many research fields. As one of the most widely used optimization algorithms, the theoretical basis and application practice of PSO are quite mature, and it is often used as a standard to measure the performance of other optimization algorithms.

4.2 Performance Testing

F1 and F2 are Sphere and Quartic functions respectively. Their mathematical expressions, search intervals, minimum values and other information are detailed in Table 1 and the function graph is shown in Fig. 2.

Figure 3 is the convergence curve of PSO, FTTA and VFTTA. In the process of F1 and F2 functions, VFTTA (red) has obvious advantages in the early iteration of the algorithm, namely, small fitness value and fast convergence speed. Table 2 is the optimization results of PSO, FTTA and VFTTA. The results in the table show that the optimization results of VFTTA are significantly better than those of the other two algorithms.

Table 1. Standard test function F1 and F2 information.

Function	Function Expression	Dimension	Search Interval	Minimum Value
F_1 (Sphere)	$F_1(x) = \sum_{i=1}^{30} x_i^2$	30	[−100,100]	0
F_2 (Quartic)	$F_2(x) = \sum_{i=4}^{30} ix_i^4 + random[0,1]$	30	[−1.28,1.28]	0

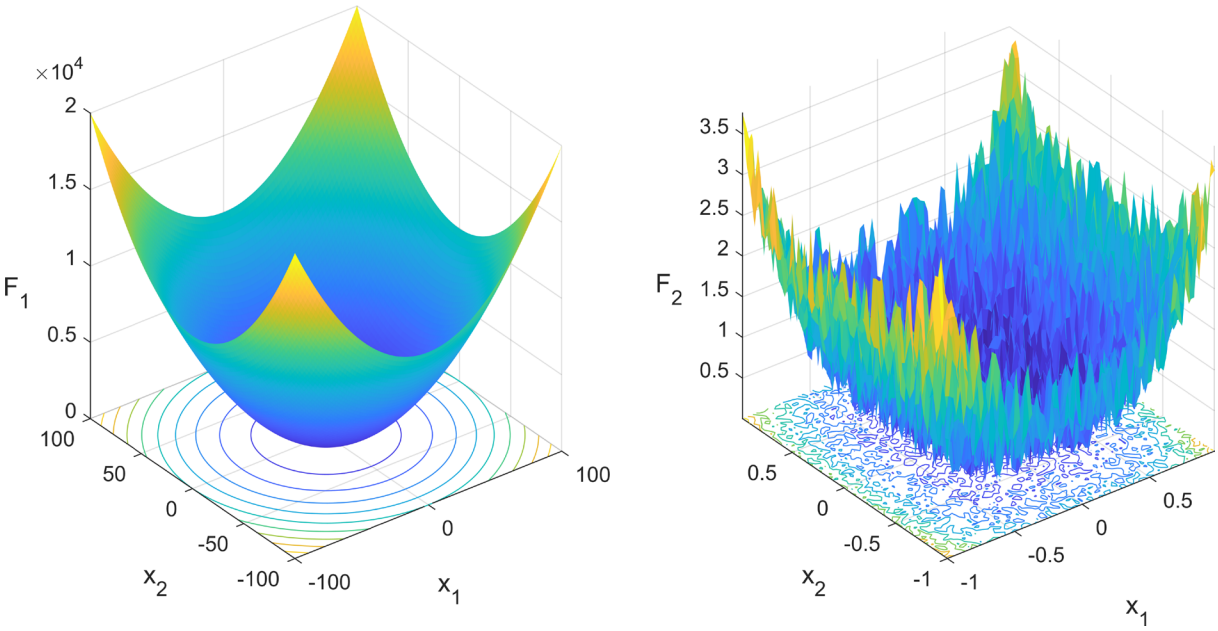

Figure 2. Images of test functions F1 (left) and F2 (right).

Table 2. Optimization results of PSO, FTTA and VFTTA.

Test Function	Extreme value	PSO			FTTA			VFTTA		
		Optimal	Mean	Standard Deviation	Optimal	Mean	Standard Deviation	Optimal	Mean	Standard Deviation
F_1	0	23.81	36.96	9.53	-6.17×10^{-6}	-9.13×10^{-7}	-1.88×10^{-6}	-2.14×10^{-13}	-2.35×10^{-14}	-6.72×10^{-14}
F_2	0	1.27	3.38	2.55	-1.96×10^{-1}	-1.38×10^{-1}	-4.17×10^{-2}	-9.60×10^{-2}	-5.57×10^{-2}	3.21×10^{-2}

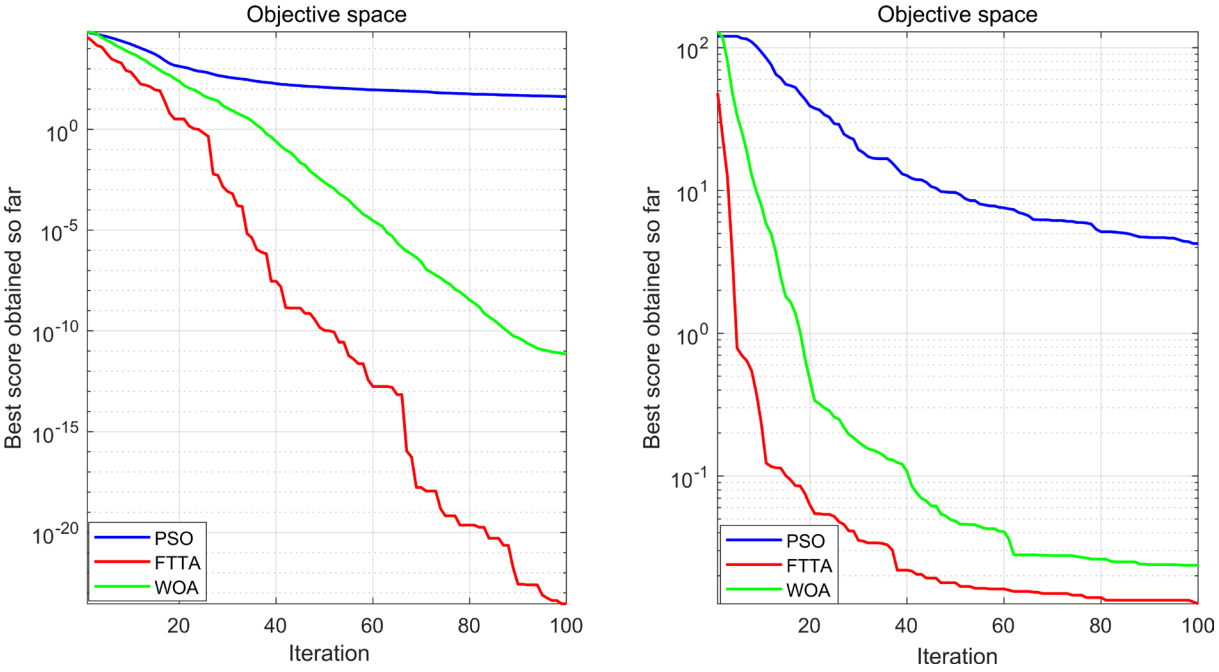

Figure 3. Convergence curves of test functions F1 (left) and F2 (right).

5. Theoretical model testing

There are many problems in the process of Rayleigh wave acquisition, so the quality of the algorithm must not be limited to the test function stage. For this reason, a common geological model is established, and different inversion parameters are configured to assess the applicability and noise resistance of VFTTA through a series of theoretical model dispersion curve inversion applications.

5.1 Dispersion curve inversion settings

5.1.1 Objective function

In order to verify the feasibility of VFTTA in the inversion of surface wave dispersion curves, this study uses the root mean square error (RMSE) as the objective function to evaluate the goodness of fit between the two. RMSE is defined as the square root of the average of the sum of the squares of the differences between the observed values and the model predicted values. The smaller the RMSE, the closer the model prediction is to the actual observed data, and the better the inversion effect. In practical applications, the model parameters are usually optimized by minimizing

the RMSE to achieve the best inversion effect. Specifically, for the inversion of the fundamental dispersion curve, the P_1 objective function is defined as:

$$P_1 = \sqrt{\sum_{i=1}^{N} \left(v_i^{inversed} - v_i^{truth}\right)^2 / N} \tag{17}$$

where N represents the frequency number of the dispersion curve; $v_i^{inversed}$ represents the Rayleigh wave phase velocity obtained after inversion of the i-th frequency point; v_i^{truth} represents the actual Rayleigh wave phase velocity of the i-th frequency point.

5.1.2 Inversion parameters

Compared with other geological parameters, shear wave velocity and layer thickness exhibit a more significant influence on the inversion results of Rayleigh surface wave dispersion curves. Consequently, in the inversion process, only shear wave velocity and layer thickness are solved, while other parameters are assigned known values. To better align with real-world scenarios where prior information is often insufficient, a wider parameter search range is established, with the upper and lower limits of the search interval set to 50% of the true value. The algorithm parameters are configured with a population size of 30 and 100 iterations, consistent across all experiments. Given the inherent randomness of the algorithm, 20 independent inversions are performed for each theoretical model to mitigate the impact of randomness, with the average of these results adopted as the final inversion outcome. The accuracy of the inversion results is further evaluated using relative error and standard deviation as performance metrics.

5.1.3 Theoretical model

To verify the applicability and effectiveness of the algorithm in dispersion curve inversion, several common theoretical geological models are constructed, including velocity-increasing models A, models B, with low-velocity layers and models C with high-velocity layers. These models are representative of scenarios frequently encountered in practical applications. Theoretical dispersion curves are generated in this study using a dispersion curve forward algorithm based on the generalized reflection-transmission coefficient method through solution of the dispersion equation of Rayleigh surface waves in layered media. Specifically, for the three designed theoretical geological models (Model A with increasing velocity, Model B with low-velocity layer, and Model C with high-velocity layer), the elastic parameter matrix of each layer (including shear wave velocity v_s, compression wave velocity v_p, density ρ, and layer thickness H) is first constructed, and then the characteristic equation of Rayleigh wave propagation in layered media is solved by the eigenvalue method.

Given that surface wave exploration primarily targets shallow and medium-depth underground media, particularly shallow regions, the model depth is constrained to within 20 meters. The shallow geology is predominantly characterized by unsaturated clay, and the Poisson's ratio of the model is assigned a random value within the range of 0.35 to 0.4. Once the shear wave velocity and Poisson's ratio for each layer are specified, the longitudinal wave velocity of the layer can be derived using Eq. (18).

$$\frac{v_p}{v_s} = \sqrt{\frac{1-\sigma}{0.5-\sigma}} \tag{18}$$

where v_p represents the longitudinal wave velocity; v_s represents the shear wave velocity; and σ represents the Poisson's ratio.

The velocity increasing model (Model A) simulates a homogeneous sedimentary basin (such as a fluvial sedimentary sequence), where the shear wave velocity increases monotonically from 150 m/s to 400 m/s with depth (Table 3), which is consistent with the typical velocity-depth relationship under stress compaction. The layer thickness parameter (4 m → 6 m) reflects the change of sedimentary cycles, and the density is uniformly

taken as 2 g/cm^3 to characterize sandy clay, which is used to verify the basic inversion ability of the algorithm in uniform strata. The model with low-velocity layer (Model B) depicts shallow soft interlayers (such as cavities or water-bearing fracture zones). The shear wave velocity of the second layer is 160 m/s, which is significantly lower than that of the adjacent layers (220→320 m/s). The Poisson's ratio of 0.35-0.4 reduces the longitudinal wave velocity to 347 m/s (v_p/v_s≈2.17), which is consistent with the characteristics of water-bearing loose sediments. The model induces dispersion curve distortion through a 3 m thick low-velocity layer (as shown in Fig. 4b1) to specifically test the algorithm's recognition sensitivity of low-velocity abnormal geological bodies. The high-speed layer model (Model C) targets bedrock uplift areas or cemented strata. The shear wave velocity of the second layer is 330 m/s, forming a high-speed anomaly (higher than the first layer 140 m/s and the third layer 240 m/s). Its longitudinal wave velocity of 848 m/s (v_p/v_s≈2.57) corresponds to the typical response of calcareous cemented conglomerate. This model causes the dispersion curve to bulge upward through the velocity inversion structure (as shown in Fig. 4c1), which effectively verifies the algorithm's ability to analyze complex structures.

The calculation of Rayleigh wave dispersion curve is based on the theory of elastic wave propagation in layered media. Given the shear wave velocity v_s, longitudinal wave velocity v_p, thickness H and density ρ of each layer, the relationship between the phase velocity v_r and the frequency f can be obtained by solving the characteristic frequency equation.

The core of the calculation process is the propagation matrix method. For the angular frequency $\omega = 2\pi f$, the propagation matrix $\mathbf{A}_j$ of each layer contains the compression wave number and shear wave number are as follows:

$$k_p = \omega\sqrt{\frac{1}{v_p^2} - \frac{1}{v_r^2}}$$
$$k_s = \omega\sqrt{\frac{1}{v_s^2} - \frac{1}{v_r^2}} \quad (19)$$

Table 3. Geological parameters and inversion search intervals of models A, B, and C.

Model	Layer	Model parameters				Search Scope	
		v_s (m/s)	v_p (m/s)	ρ (g/cm^3)	H (m)	v_s (m/s)	H (m)
A	1	150	335	2	4	75~225	2~6
	2	200	471	2	5	100~300	2.5~7.5
	3	300	641	2	6	150~450	3~9
	4	400	1077	2	∞	200~600	∞
B	1	220	491	2	3	110~330	1.5~4.5
	2	160	347	2	5	80~240	2.5~7.5
	3	320	740	2	5	160~480	2.5~7.5
	4	420	1198	2	∞	210~630	∞
C	1	140	330	2	3	70~210	1.5~4.5
	2	330	848	2	6	165~495	3~9
	3	240	525	2	4	120~360	2~6
	4	440	1256	2	∞	220~660	∞

The overall propagation matrix is obtained by multiplying the matrices of each layer:

$$\mathbf{A} = \prod_{j=N}^{1} \mathbf{A}_j(h_j) \tag{20}$$

where $\mathbf{A}_j(z)$ specific form is:

$$\mathbf{A}_j(z) = \begin{bmatrix} e^{-ik_p z} & 0 & 0 & 0 \\ 0 & e^{-ik_s z} & 0 & 0 \\ 0 & 0 & e^{ik_p z} & 0 \\ 0 & 0 & 0 & e^{ik_s z} \end{bmatrix} \tag{21}$$

The solution of the characteristic equation det(A) = 0 is the Rayleigh wave phase velocity. In the actual VS calculation, first determine the reasonable velocity search range [0.5 min(v_p), 1.5 max(v_s)], and then solve the equation by numerical method. For each frequency point, start the search from the lowest order mode and gradually find possible higher order modal solutions.

5.1.4 Adding noise

The models established above are all in an ideal state without any noise. However, in the actual data collection, the surface wave often contains a certain amount of random noise. When the noisy surface wave signal is converted into a dispersion energy diagram, the dispersion curve will have a certain range of disturbances, resulting in a certain error in the extracted dispersion curve, which will affect the optimization ability of the inversion algorithm and reduce the accuracy of the inversion results. To test and evaluate the anti-noise performance of the algorithm, 10% random noise is introduced to the three established theoretical models. The mathematical equation for adding noise is as follows:

$$v_r^{noisy} = v_r^{truth} + d \times \frac{\sum_{i=1}^{N} v_{r,i}^{truth}}{N} \times (rand_1 - rand_2) \tag{22}$$

where v_r^{noisy} represents the dispersion curve (phase velocity) after adding noise; v_r^{truth} represents the real dispersion curve; d represents the percentage content of added noise, which is taken as 0.1 in this test; $v_{r,i}^{truth}$ represents the i real dispersion curve of the dispersion curve, and $rand_1$ and $rand_2$ represent the random numbers generated each time.

5.2 Dispersion curve inversion analysis

5.2.1 Noise-free fundamental-order dispersion curve inversion

In this section, VFTTA, FTTA and PSO are applied to the inversion of the noiseless fundamental mode dispersion curve of models A, B and C respectively. Combined with the advantageous range of surface wave energy concentration in actual engineering applications, the frequency is set to 3~60 Hz, the frequency interval is 2 Hz, and there are 29 frequency points in total. In the inversion parameters, the population number of VFTTA, FTTA and PSO algorithms is set to 30, and the number of iterations is all set to 100. In order to avoid the influence of random factors in the algorithm on the inversion results, each theoretical model test is independently inverted 20 times, and the initial model is randomly generated for each inversion. Finally, the mean output of 20 times is used as the inversion result, and the standard deviation result of 20 inversion data is used as an indicator to measure the stability of the algorithm.

The results of inverting the noiseless fundamental mode dispersion curve using three algorithms are shown in Fig. 4. From the inversion results shown in Fig. 4, it can be seen that the three algorithms can fit the dispersion curve well. However, from the observation of the inverted shear wave velocity model, it can be seen that no matter which of the three models is used, the shear wave velocity model obtained by VFTTA inversion (the red solid line in Fig. 3b, d and e) can be well matched with the theoretical shear wave velocity model (the black solid line in Fig. 4b, d and e), and the shear wave velocity model obtained by FTTA and PSO inversion (the blue and pink solid lines in Fig. 4b, d and e) has a certain deviation from the theoretical model. This phenomenon that the dispersion curve has a high degree of fitting, but the inverted model parameters have a certain deviation also reflects the multi-solution and

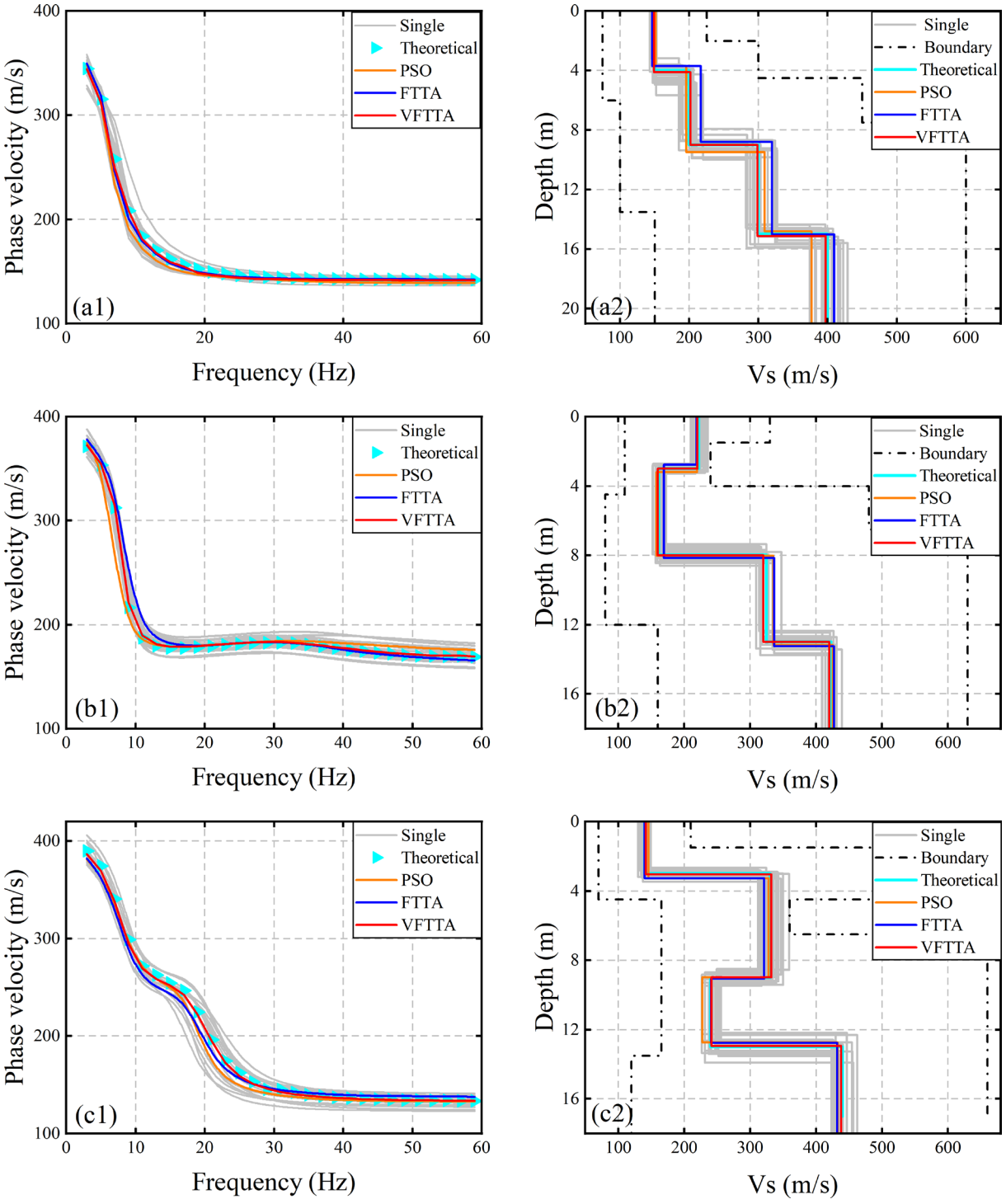

Figure 4. Inversion results of noise-free data for models A, B and C.

non-uniqueness of the surface wave dispersion curve inversion and further verifies the excellent performance of VFTTA in solving the dispersion curve inversion problem.

The first column of Fig. 6 shows the iterative convergence process of the noise-free dispersion curve inversion by FTTA, VFTTA and PSO algorithms, and all vertical axes are displayed in logarithmic form. The convergence speeds of the three algorithms are similar, but in terms of the final convergence error, the results obtained by VFTTA for processing the three model data are significantly lower than those of the other two algorithms. The convergence performance of VFTTA is also consistent with the high degree of fit of the inverted structure in Fig. 4. In addition, if the convergence speed of the algorithm is fast but the convergence error is high, it also indicates that the algorithm has a "premature" problem with global optimization, that is, the solution converges to a local extreme value, indicating that the algorithm performance is poor.

In order to avoid redundant display, Table 3 only gives the mean results, standard deviations and relative errors of each model parameter obtained by VFTTA inversion of noise-free dispersion data. The maximum relative error of the parameters obtained by VFTTA inversion for the three models is only 2.00%, the maximum standard deviation of v_s is 2.71 m/s, and the maximum standard deviation of h is 0.08 m. After calculation, the maximum relative errors in the model parameters obtained by FTTA and PSO inversion are 4.23% and 7.46%, the maximum v_s standard deviation is 6.28 m/s and 14.74 m/s, and the maximum h standard deviation is 0.18 m and 0.25 m. The maximum relative error and maximum standard deviation of the model parameters obtained by VFTTA inversion are significantly lower than the inversion results obtained by FTTA and PSO. In addition, the standard deviation of the parameters obtained by 20 independent VFTTA inversions shows that the overall deviation of the 20 independent inversions is low, that is, the stability of the VFTTA algorithm is high (see Table 4). The above results show that VFTTA can accurately and stably invert the theoretical noise-free Rayleigh wave dispersion curve; compared with FTTA and PSO, VFTTA has stronger optimization performance and can better approach the global optimal solution.

5.2.2 Inversion of the noisy fundamental order dispersion curve

The three algorithms are used for the inversion of noisy data of the three models, and the parameters set for the inversion are consistent with those for the noise-free processing. The inversion results are shown in Fig. 5. As can be seen from Fig. 5, after adding noise to the dispersion curve, the dispersion curve obtained by VFTTA inversion can still fit the noise-free dispersion curve of the theoretical model well, and the other two algorithms also obtain good fitting effects. However, the shear wave velocity model inverted by the three algorithms is more obviously different from the theoretical model. The direct reason for this phenomenon is the addition of noise data. But overall, VFTTA still has the best model inversion result.

The second column of Fig. 6 further shows the iterative convergence process of the FTTA, VFTTA and PSO algorithms when inverting the noisy dispersion curve, and all y axes are also displayed in logarithmic form. At this time, the convergence errors of the FTTA, VFTTA and PSO algorithms are significantly higher than those obtained when inverting the noise-free data. However, the convergence speeds of the three algorithms are still relatively consistent. VFTTA still maintains the lowest fitting error.

From the perspective of iteration speed and convergence, the noisy model A (Fig. 6 (a2)) shows that VFTTA reaches a stable error level in the early iterations (<20 generations) (the RMSE of the noise-free model Model A drops to 5 m/s at 15 generations), while FTTA and PSO need more than 35 generations to achieve the same accuracy. The convergence curves of the three models all show that the RMSE obtained by PSO and FTTA is higher than that of VFTTA, which means that the algorithm has fallen into premature convergence. Experiments verify that VFTTA has better ability to avoid premature convergence and jump out of local optimality than PSO and FTTA.

Further, from the results of VFTTA inversion of noisy dispersion data given in Table 4, it can be seen that when there is noise in the input data, the relative error and standard deviation in the inversion results mostly increase. However, compared with FTTA, VFTTA and PSO algorithms, the VFTTA algorithm still maintains the best inversion effect. Compared with PSO and FTTA, VFTTA can more accurately identify layer thickness and shear wave velocity, and its inversion results are closer to the real model.

From Table 4, in the inversion of 100 iterations, the standard deviation of VFTTA is significantly lower: the standard deviation of shear wave velocity and the standard deviation of layer thickness parameters of VFTTA are lower than those of FTTA and PSO, which shows that VFTTA has stronger resistance to random interference and higher repeatability of inversion results.

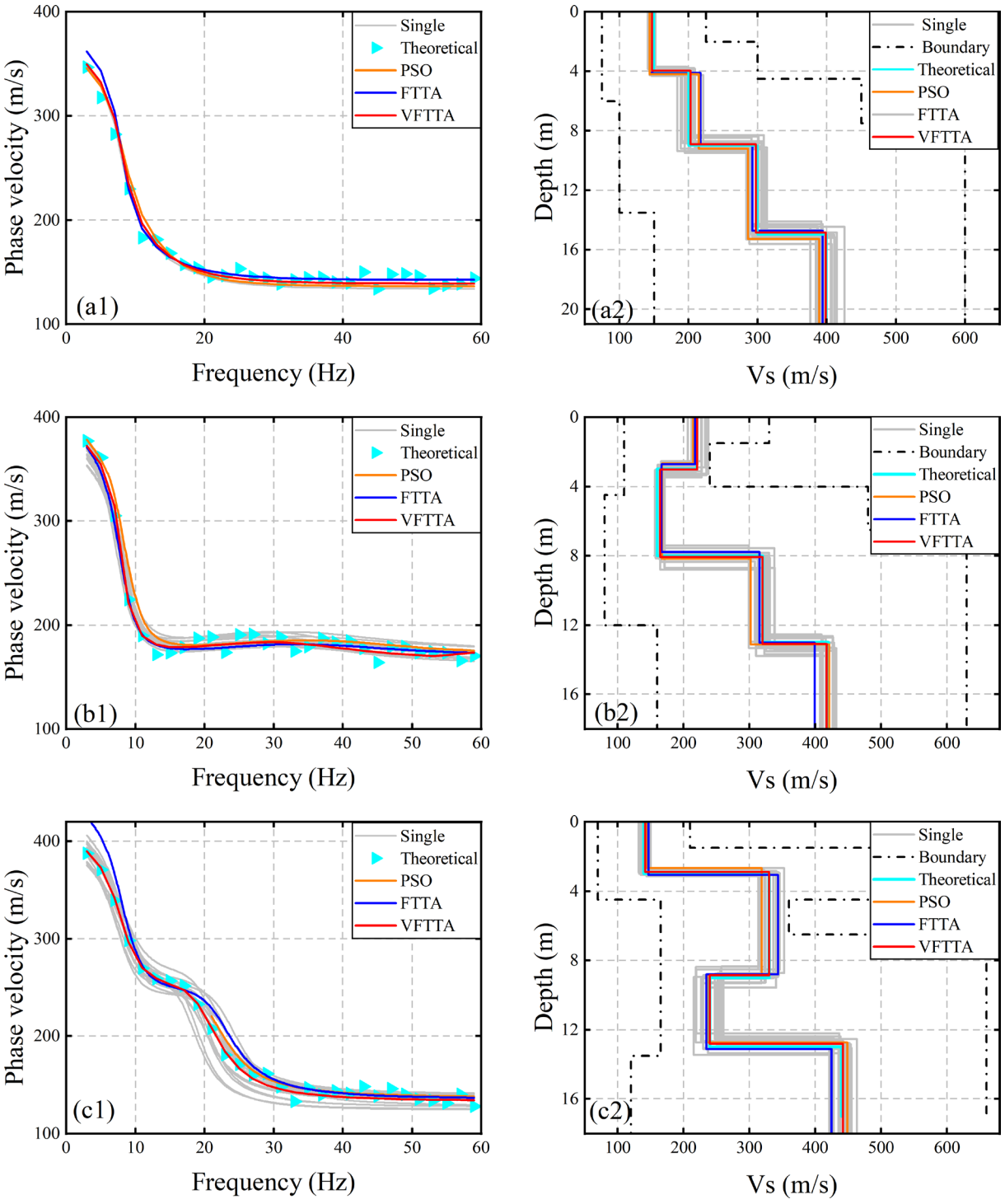

Figure 5. Inversion results of noisy data for models A, B and C.

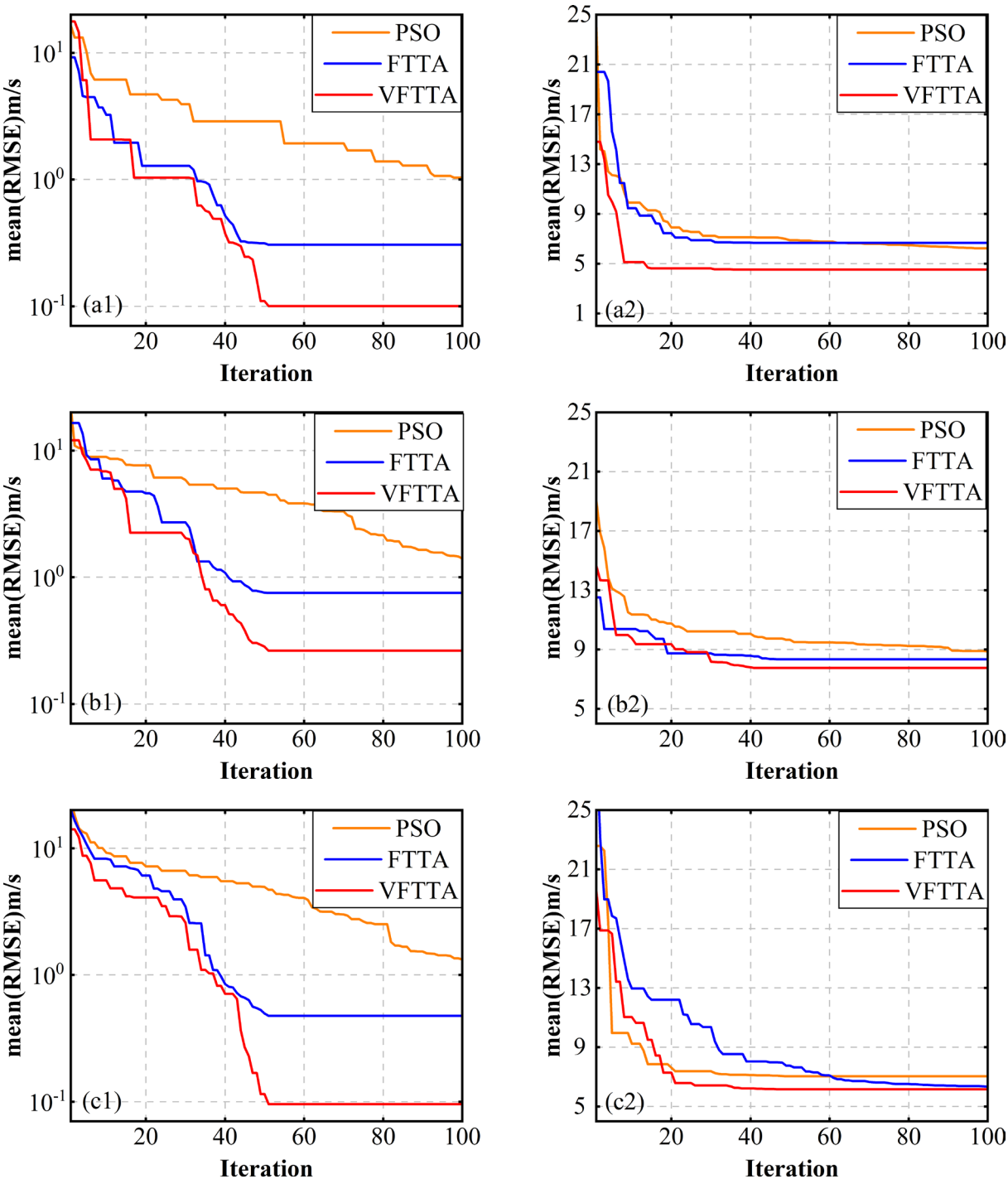

Figure 6. The iterative process of VFTTA, FTTA and PSO when inverting dispersion data with and without noise.

In terms of noise resistance, the VMD-FTTA preprocessing system separates noise adaptively through IMF energy entropy, improves the signal-to-noise ratio from the signal source, and enables VFTTA to maintain high accuracy after adding 10% noise. Whether in terms of shear wave velocity, layer thickness or RMSE convergence curve, the algorithm performance is better.

The above results show the superior performance of VFTTA, which has a wider application potential in the dispersion curve inversion of complex geological models.

Table 4. VFTTA inversion results with and without noise for models A, B and C.

Model	Parameter	True value	Noise-free			Noise-containing		
			Mean	Relative error	Standard Deviation	Mean	Relative error	Standard Deviation
Model A	$v_{s1}/(m{\cdot}s^{-1})$	150	149.07	0.62	2.62	147.07	1.95	3.15
	$v_{s2}/(m{\cdot}s^{-1})$	200	202.05	1.03	10.72	202.93	1.47	10.46
	$v_{s3}/(m{\cdot}s^{-1})$	300	298.84	0.39	10.44	297.34	0.89	9.75
	$v_{s4}/(m{\cdot}s^{-1})$	400	398.66	0.34	12.37	397.02	0.75	15.67
	$h_1/(m)$	4	3.98	0.50	0.20	4.12	3.00	0.29
	$h_2/(m)$	5	4.92	1.60	0.23	4.87	2.60	1.12
	$h_3/(m)$	6	5.92	1.33	0.26	6.15	2.50	1.16
Model B	$v_{s1}/(m{\cdot}s^{-1})$	220	221.74	0.79	8.61	223.37	1.53	8.29
	$v_{s2}/(m{\cdot}s^{-1})$	160	161.37	0.86	5.62	164.46	2.79	4.04
	$v_{s3}/(m{\cdot}s^{-1})$	320	319.98	0.01	10.48	322.41	0.75	12.2
	$v_{s4}/(m{\cdot}s^{-1})$	420	422.71	0.65	7.20	417.34	0.63	9.94
	$h_1/(m)$	3	2.94	2.00	0.20	3.11	3.67	0.28
	$h_2/(m)$	5	4.97	0.60	0.28	4.93	1.40	0.24
	$h_3/(m)$	5	5.03	0.60	0.21	5.12	2.40	0.29
Model C	$v_{s1}/(m{\cdot}s^{-1})$	140	141.68	1.20	5.48	142.21	1.58	3.82
	$v_{s2}/(m{\cdot}s^{-1})$	330	329.92	0.02	13.43	332.16	0.65	19.60
	$v_{s3}/(m{\cdot}s^{-1})$	240	240.10	0.04	10.22	241.31	0.55	17.93
	$v_{s4}/(m{\cdot}s^{-1})$	440	441.74	0.40	11.55	437.95	0.47	20.03
	$h_1/(m)$	3	3.06	2.00	0.16	2.89	3.67	0.21
	$h_2/(m)$	6	5.92	1.33	0.29	5.96	0.67	0.24
	$h_3/(m)$	4	3.97	0.75	0.29	3.96	0.10	0.37

5.3 Joint inversion of high-order dispersion curves

When surface waves propagate in some special strata, high-order modes may dominate. If the dispersion curves of the fundamental mode and the high-order mode are combined for inversion, the constraints on the inversion results can be strengthened and the accuracy of the inversion results can be improved. In this section, the fundamental dispersion curve of model B and the first- and second-order high-order dispersion curves are combined to perform inversion tests on PSO, FTTA and VFTTA. The noise-free and noise-containing inversion cases are also considered. Since the VFTTA algorithm has a very excellent performance in the fundamental mode inversion, in order to further increase the difficulty, the model parameter search range is still set to ±50%, and the other parameters involved in the inversion of the three algorithms are consistent with the previous test. The dispersion curve fitting results, the shear wave velocity profile fitting results and the corresponding convergence curves are shown in Fig. 7.

It can be seen that after expanding the model space, but at the same time adding high-order dispersion information, the PSO, FTTA and VFTTA algorithms still maintain a good dispersion curve fitting effect, whether considering or not considering the addition of noise. However, in terms of inverted shear wave velocity profiles, VFTTA achieved the best fitting result compared with the other two algorithms. The inversion mean, standard deviation and relative error of VFTTA are shown in Table 5. It can be verified that the use of multi-order dispersion curves for inversion can indeed make the inversion results more accurate and reliable, but the optimization algorithm with stronger inversion performance always has the best inversion output.

Table 5. VFTTA joint inversion results of multi-order dispersion curves with and without noise for model B.

Model	Parameter	True value	Noise-free			Noise-containing		
			Mean	Relative error	Standard Deviation	Mean	Relative error	Standard Deviation
Model B	$v_{s1}/(\mathrm{m\cdot s^{-1}})$	220	217.95	0.93	7.67	222.99	1.36	9.87
	$v_{s2}/(\mathrm{m\cdot s^{-1}})$	160	161.51	0.94	9.99	163.24	2.03	7.31
	$v_{s3}/(\mathrm{m\cdot s^{-1}})$	320	322.76	0.86	14.45	325.66	1.77	15.01
	$v_{s4}/(\mathrm{m\cdot s^{-1}})$	420	421.51	0.36	3.25	421.64	0.39	6.22
	$h_1/(\mathrm{m})$	3	3.09	3.00	0.26	3.09	3.00	0.29
	$h_2/(\mathrm{m})$	5	4.86	2.80	0.37	5.10	2.00	0.31
	$h_3/(\mathrm{m})$	5	5.02	0.40	0.31	5.08	1.60	0.30

In the theoretical tests, we have a known theoretical dispersion curve. To simulate uncertainty in real life, we introduce disturbances to the known information. This step is intended to test the interference resistance and stability of the inversion algorithm kernel itself, to verify whether FTTA can still stably invert a velocity model close to the real one even if the extracted dispersion curve has errors. Although the objects of noise addition differ, this experiment aims to demonstrate that once the quality of the dispersion curve is improved through VMD (i.e., reducing the input errors), the accuracy of the inversion results can be significantly enhanced. This provides a theoretical basis for the necessity of VMD in processing actual data.

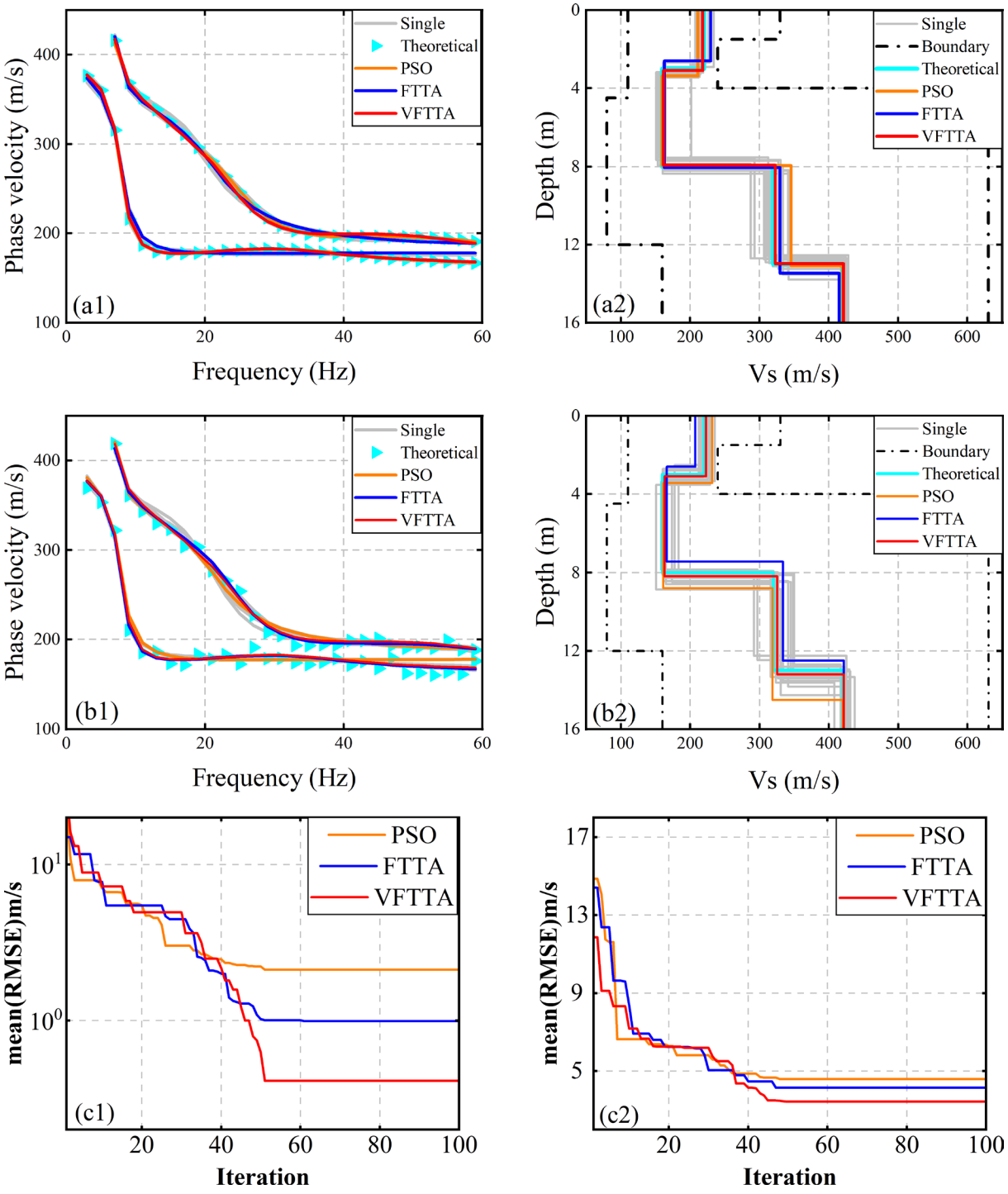

Figure 7. Inversion results of multi-mode dispersion curves of model B (a) Model B noise-free multi-order dispersion data (black solid line) and inverted dispersion curves (PSO: pink solid line; FTTA: blue solid line; VFTTA: red solid line).

6. Actual data test

To verify the practicality of VFTTA, measured micromotion data from a specific area in Nanjing is selected for inversion testing. The observation started at 22 November 2023, 10:30:00, and the acquisition time was 45 minutes. A 5 Hz node instrument was used, the sampling interval was 2 ms, and the track spacing was 2 m. There was a set of borehole data containing shear wave velocity around the measuring point for verification as shown in Fig. 10. Figure 8 shows the original micromotion data collected. After the dispersion analysis of the Rayleigh surface wave data, the dispersion energy spectrum is obtained as shown in Fig. 8(b), and the fundamental dispersion curve extracted from the dispersion energy spectrum is shown in Fig. 8(b). From the blue part of the low-frequency area in the dispersion diagram 8(b), it can be seen that there is a low-velocity layer, which may be caused by geological layers such as loose soil layers or saturated soft soil. By analyzing the dispersion curve and velocity profile in Fig. 8(b), the wave velocity distribution information of the stratum can be obtained, and then the stratigraphic structure and physical properties at different depths underground can be inferred. The parameters used in the inversion calculation are set based on the known borehole information. The shallow stratigraphic structure of the measuring point can be divided into five layers, including low-velocity interlayers, which better approximates the real complex stratigraphic structure and verifies the practicality of the algorithm. The inversion parameters and search range are shown in Table 6.

In practical data applications, we only have the original field seismic recordings (time-domain signals). From the noisy, multimodal coupled raw signals, we extract high-fidelity target modal dispersion curves. This is the prerequisite for the entire inversion success and is the most critical difficulty. Here, the VMD-FTTA system plays its most complete and essential role. FTTA first optimizes the VMD parameters, then VMD decomposes and reconstructs the time-domain seismic records, directly removing time-domain noise and separating modes, thus obtaining a purer signal and ultimately extracting more accurate dispersion curves. The ultimate goal is to obtain a reliable underground speed model. The final goals of both paths are completely identical – obtaining a high-precision speed model. The theoretical data path verified the principle that “quality input is crucial for inversion results,” while

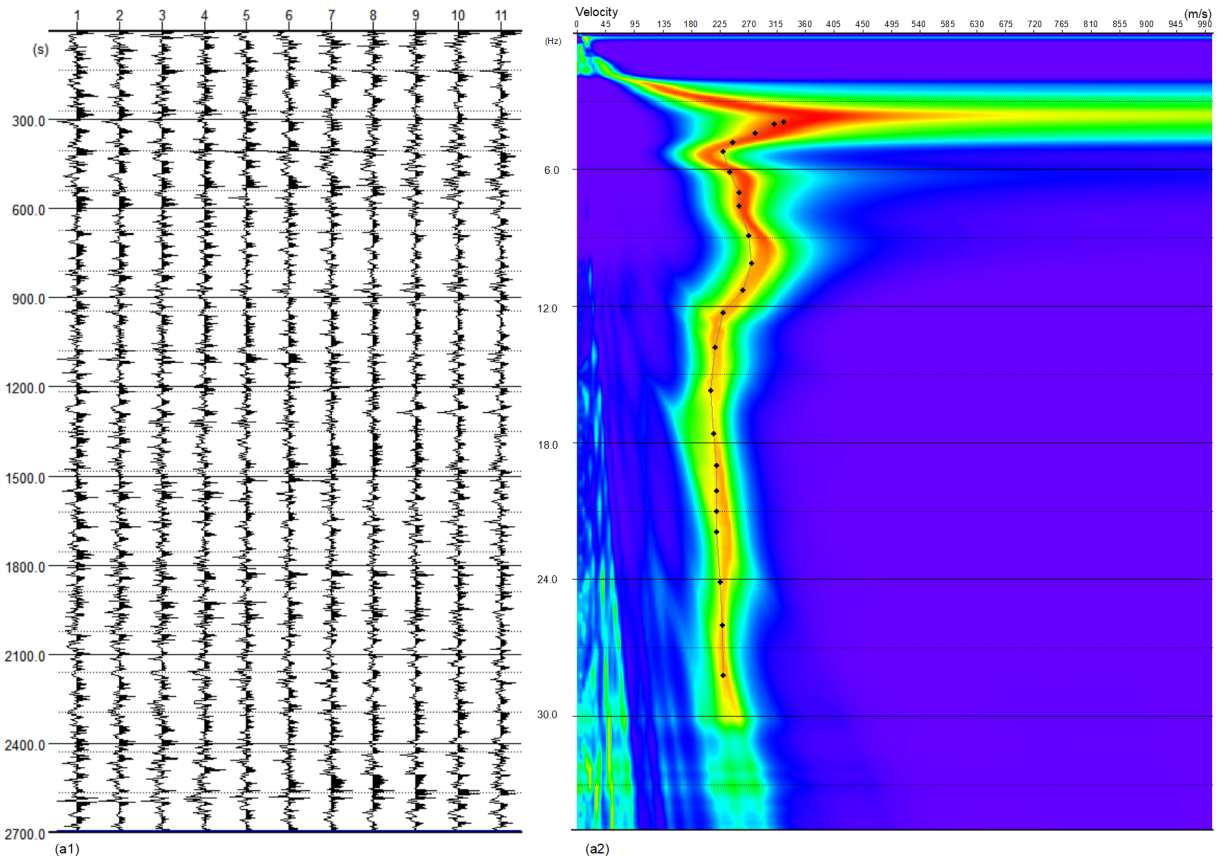

Figure 8. Measured Rayleigh surface wave data (a) and dispersion spectrum (b).

the practical data path demonstrated how we utilize the VMD-FTTA system to create such "quality input" from scratch. The two complement each other, together proving the effectiveness and practicality of our method.

Table 6. Actual data inversion parameter settings.

Layer number	Model parameters		Search Scope	
	Poisson's ratio	ρ (g/cm^3)	v_s (m/s)	H (m)
1	0.30	1.8	100~500	1~5
2	0.30	2.0	50~350	1~5
3	0.35	2.1	300~700	1~5
4	0.35	2.1	100~500	1~5
5	0.42	2.1	100~500	1~5

As can be seen from Fig. 9(a1), VFTTA (red solid line) and FTTA (light blue solid line) perform well in the fitting effect of dispersion curves and can match the actual data (black solid line) well. Especially in the low frequency band (0-10 Hz), the fitting curves of the three algorithms are almost overlapped, indicating the consistency of the algorithms in fitting low-frequency data. From the inversion results of the shear wave velocity model, the shear wave velocity profile generated by VFTTA has high accuracy in identifying the thickness and velocity changes of each layer and has a good overall fit with the actual model (black solid line), especially in the shallow layer (0-8 meters) and the medium-deep layer (12-24 meters). The curve inverted by VFTTA is closely close to the actual shear wave velocity. In contrast, PSO and FTTA show certain deviations in identifying the layer interface at a depth of 12 meters and 20 meters. PSO deviates slightly from the actual drilling data overall, and PSO shows a trend of low fitting in deep layers (below 12 meters). In summary, VFTTA has good practicality in the inversion of this set of data. Therefore, VFTTA not only performs well in the inversion of Rayleigh wave dispersion curves but also has the potential to be extended to solve other geophysical inversion problems.

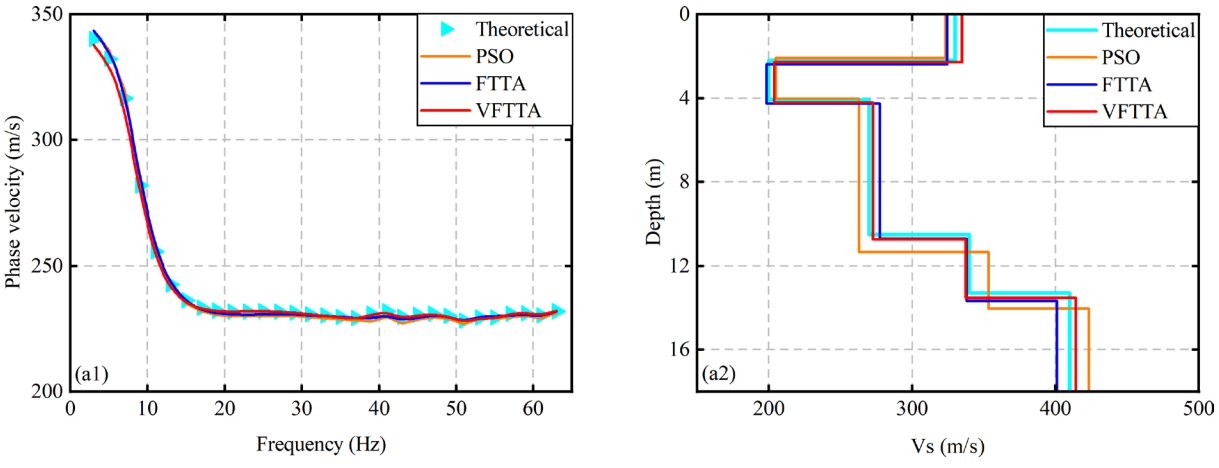

Figure 9. Inversion results of Rayleigh surface wave dispersion curves from example data (a1 is the dispersion curve, a2 is the shear wave velocity profile, the yellow, dark blue and red solid lines are PSO, FTTA and VFTTA respectively).

Layer Bottom Depth（m）	Layer Thickness（m）	Bar Chart (1：200)	Geotechnical Description
2.20	2.20		Miscellaneous fill: Primarily composed of piled cohesive soil, with cultivated soil at the bottom.
4.10	1.90		Silty clay: Plastic; high toughness; high strength.
10.50	6.40		Round gravel: Saturated, slightly dense, mostly sub-rounded gravel, filled with sand.
13.30	2.80		Clayey breccia: Saturated and loose, containing approximately 30%–40% clayey soil.
21.80	8.50		Gravelly clay: Saturated, fluid-plastic, containing approximately 20%–30% gravel.

Figure 10. Presents the logging data.

7. Conclusion

The Football Team Training Algorithm (FTTA) is introduced and further improved for application in the inversion of surface wave dispersion curves. A complex benchmark function test and different geological models (no noise and with different degrees of noise) and measured micro-seismic data are set up to apply the algorithm to verify the practicality, stability, applicability and noise resistance of the algorithm. The following conclusions are drawn:

(i) In the test of two complex functions, VFTTA can effectively avoid falling into the local optimal solution. In the later stage of iteration, compared with PSO, FTTA is closer to the theoretical extreme value of the function. It can be seen that VFTTA has a strong global search ability and can be used in dispersion curve inversion.

(ii) There are indeed many noise problems in the process of Rayleigh wave acquisition, so an algorithm with good noise resistance is needed. In the dispersion curve inversion of three theoretical models, VFTTA can accurately invert the shear wave velocity and layer thickness within a large parameter search range, and the inversion results are very close to the theoretical model. Therefore, it shows that VFTTA has good applicability and noise resistance in the inversion of different theoretical models.

(iii) The inversion results of measured data show that, in the same search space, compared with PSO and FTTA, the inversion results of VFTTA are more consistent with the borehole data and have higher inversion accuracy. This proves that VFTTA has good practicality and also shows that VFTTA has good development potential and broad development space in the field of surface wave inversion.

Acknowledgements. This work was funded by the Youth Project of the Jiangxi Provincial Natural Science Foundation (20252BAC200265, 2023BAB213079), the Youth Project of the National Natural Science Foundation [42474197, 42004113], the Key Project of the Jiangxi Provincial Natural Science Foundation (20242BAB26049), the "Leadership in Research" project of the Nuclear Geoscience Department of Donghua University (2024HDX07), the Gan-Po Talent Support Program - Key Academic and Technical Leader Training Project (20243BCE51012), the Joint Innovation Fund Project of the China National Nuclear Corporation - National Key Laboratory for Nuclear Resources and Environment (East China University of Technology) [2023NRE-LH-08], Jiangxi Provincial College Student Innovation and Entrepreneurship Project [S202410405015], and the Jiangxi Provincial Graduate Innovation Special Fund Project YC2024-8492.

References

Ai, D. H. and Q. Q. Cheng (2009). Estimation of 2D s-wave velocity section with low velocity layers by OCCAM algorithm, Geotechnical Investigation and Surveying, 37, 4, 87-90.

Beaty, K. S., D. R. Schmitt and M. Sacchi (2002). Simulated annealing inversion of multimode Rayleigh wave dispersion curves for geological structure, Geophys. J. Int., 151, 2, 622-631, doi:10.1046/j.1365-246X.2002.01809.x.

Bhattacharya, S. N. (2015). Sensitivities of surface wave velocities to the medium parameters in a radially anisotropic spherical Earth and inversion strategies, Ann. Geophys., 58, 5, S0545, doi:10.4401/ag-6806.

Dal Moro, G., M. Pipan and P. Gabrielli (2007). Rayleigh wave dispersion curve inversion via genetic algorithms and marginal posterior probability density estimation, J. Appl. Geophys., 61, 1, 39-55, doi:10.1016/j.jappgeo.2006.04.002.

Dorman, J. and M. Ewing (1962). Numerical inversion of seismic surface wave dispersion data and crust-mantle structure in the New York-Pennsylvania area, J. Geophys. Res., 67, 13, 5227-5241, doi:10.1029/JZ067i013p05227.

Fu, Y. Y. and Y. Gao (2016). Phase velocity tomography of Rayleigh and Love waves using ambient noise in Northeast China, Chin. J. Geophys., 59, 2, 494-503, doi:10.6038/cjg20160209.

Fu, Y., A. Hanbing, Z. A. Yao, Z. X. Mei et al. (2023). Inversion of the Rayleigh wave dispersion curves based on the sine-cosine algorithm, Geophysical and Geochemical Exploration, 47, 6, 1467-1478, doi:10.11720/wtyht.2023.1239.

Hashim, F. A. and A. G. Hussien (2022). Snake Optimizer: A novel meta-heuristic optimization algorithm, Knowl. Based Syst., 242, 108320, doi:10.1016/j.knosys.2022.108320.

Hou, J., Y. Cui, M. Rong and B. Jin (2024). An Improved Football Team Training Algorithm for Global Optimization, Biomimetics, 9, 7, 419, doi:10.3390/biomimetics9070419.

Hu, X. and R. Eberhart (2002). Solving constrained nonlinear optimization problems with particle swarm optimization, Proceedings of the Sixth World Multiconference on Systemics, Cybernetics and Informatics, Citeseer, 203-206.

Kennedy, J. and R. Eberhart (1995). Particle swarm optimization Proceedings of ICNN'95 International Conference on Neural Networks, IEEE, 4, 8, 1942-1948, doi:10.1109/ICNN.1995.488968.

Li, H. L., X. G. Tuo and X. H. Jiang (2017). A finite difference simulation method for multi-wave exploration in complex mountainous areas, Science Technology and Engineering, 17, 23.

Liu, G. X., H. Y. Shen and H. Che (2023). Inversion of Rayleigh wave dispersion curve via adaptive logarithmic Spiral-Lévy firefly algorithm, Chin. J. Geophys., 66, 7, 3011-3025, doi:10.6038/cjg2022Q0558.

Li, W. G., H. Wu and X. X. Huang (2024). Unmanned aerial vehicle path planning method based on football team training algorithm, International Conference on Computer Information Science and Application Technology (CISAT), Hangzhou, China, 25-29, doi:10.1109/CISAT62382.2024.10695324.

Li, X. and Q. Li (2016). Near-Surface Ambient Noise Tomography in the Baogutu Copper Deposit Area, J. Geophys. Eng., 13, 868-874, doi:10.1088/1742-2132/13/6/868.

Liu, S., H. Shen, H. Che, B. Wang et al. (2025). Inversion of Rayleigh wave dispersion curves integrating the Osprey – Cauchy and Pigeon-inspired optimization algorithm, Acta Geophys., 73, 3195-3212, doi:10.1007/s11600-025-01553-1.

Martínez, M. D., X. Lana, J. Olarte, J. Badal et al. (2000). Inversion of Rayleigh wave phase and group velocities by simulated annealing, Phys. Earth Planet. Inter., 122, 1-2, 3-17, doi:10.1016/S0031-9201(00)00183-7.

Nematollahi, A., A. Rahininejad and B. Vahidi (2017). A novel physical based meta-heuristic optimization method known as lightning attachment procedure optimization, Appl. Soft Comput., 59, 596-621, doi:10.1016/j.asoc.2017.06.033.

North, R. G. and C. R. D. Woodgold (1994). Automated detection and association of surface waves, Ann. Geophys., 37, 3, doi:10.4401/ag-4208.

Park, C. B., R. D. Miller and J. Xia (1999). Multichannel analysis of surface waves (MASW), Geophysics, 649, 659-992, doi:10.1190/1.1444590.

Pei, J. Y., S. M. Chen and Z. K. Liu (1994). Inversion of near surface low velocity zone parameter, Prog. Geophy.,16, 1, 89-92.

Peng, W. S., H. P. Li, Y. J. Gu, L. Shi et al. (2025). An improved meta-heuristic optimization algorithm based on chaotic mapping inspired by the football team training, International Conference on Robotics, Intelligent Control and Artificial Intelligence (RICAI), Nanjing, China, 2024, 866-870, doi:10.1109/RICAI64321.2024.10910973.

Rayleigh, L. (1885). On waves propagated along the plane surface of an elastic solid, Proceedings of the London Mathematical Society, 1, 1, 4-11, doi:10.1112/plms/s1-17.1.4.

Ren, W., Z. Yao, Z. Feng, W. Li et al. (2024). Research on the Rayleigh Surface Wave Inversion Method Based on the Improved Whale Optimization Algorithm, Ann. Geophys., 67, 1, DM104, doi:10.4401/ag-9042.

Suresh, G., S. N. Bhattacharya and S. S. Teotia (2015). Crust and upper mantle velocity structure of the northwestern Indian Peninsular Shield from inter-station phase velocities of Rayleigh and Love waves, Ann. Geophys., 58, 2, S0215, doi:10.4401/ag.12243.

Shi, Y. L. and W. Jin (1995). Gentic Algorthms Inversion of Lithospheric Structure from Surface wave Dispersion, Chin. J. Geophys., 2, 89-198.

Steeples, D. W. (2000). A review of shallow seismic methods, Ann. Geophys., 43, 6, doi:10.4401/ag-3687.

Tselentis, G. A. and G. Delis (1998). Rapid assessment of S-wave profiles from the inversion of multichannel, Ann. Geophys., 41, 1, doi:10.4401/ag-3788.

Wang, Y. (2025). An intelligent path planning algorithm for dynamic football training environments, Expert Syst. Appl., 277, 126769, doi:10.1016/j.eswa.2025.126769.

Wang, Y. M., X. H. Song and X. Q. Zhang (2021). Research on nonlinear inversion of seismic surface waves based on artificial neural network algorithm, Oil Geophys. Prospect., 56, 5, 979-991, doi:10.13810/j.cnki.issn.1000-7210.2021.05.005.

Wu, D., X. Wang, Q. Su and T. Zhang (2019). A MATLAB Package for Calculating Partial Derivatives of Surface-Wave Dispersion Curves by a Reduced Delta Matrix Method, Appl. Sci., 9, 5214, doi:10.3390/app9235214.

Xia, J. H., L. L. Gao, Y. D. Pan, S. Chao et al. (2015). New findings in high-frequency surface wave method, Chin. J. Geophys., 58, 8, 2591-2605, doi:10.6038/cjg20150801.

Xia, J. H., R. D. Miller, C. B. Park, J. A. Hunter et al. (2002). Comparing shear-wave velocity profiles inverted from multichannel surface wave with borehole measurements, Soil Dyn. Earthq. Eng., 22, 3, 181-190, doi:10.1016/S0267-7261(02)00008-8.

Xia, J. H., Y. X. Xu, Y. H. Luo, R. D. Miller et al. (2012). Advantages of using multichannel analysis of Love waves (MALW) to estimate near-surface shear-wave velocity, Surv. Geophys., 33, 5, 841-860, doi:10.1007/s10712-012-9174-2.

Xia, J. H., R. D. Miller and C. B. Park (1999). Estimation of near-surface shear-wave velocity by inversion of Rayleigh waves, Geophysics, 64, 691-700, doi:10.1190/1.1444578.

Yamanaka, H. and H. Ishida (1996). Application of genetic algorithms to an inversion of surface-wave dispersion data, Bull. Seismol. Soc. Am., 86, 2, 436-444, doi:10.1785/BSSA0860020436.

Zhang, K., B. W. Zhang, J. X. Liu and M. C. Xu (2016). Analysis on the cross of Rayleigh-wave dispersion curves in viscoelastic layered media, Chin. J. Geophys., 59, 3, 972-980, doi:10.6038/cjg20160319.

Zhang, S. and L. Chan (2003). Possible effects of misidentified mode number on Rayleigh wave inversion, J. Appl. Geophys., 53, 1, 17-29, doi:10.1016/S0926-9851(03)00014-4.

Zhang, S. X., L. S. Chan, C. Y. Chen, F. C. Dai et al. (2003). Apparent Phase Velocities and Fundamental-Mode Phase Velocities of Rayleigh Waves, Soil Dyn. Earthq. Eng., 23, 563-569, doi:10.1016/S0267-7261(03)00069-1.

***CORRESPONDING AUTHOR: Yao ZHENAN**,
Jiangxi Provincial Earthquake Disaster Mitigation and Engineering Geological Disaster Detection Engineering Research Center, East China University of Technology, Nanchang, Jiangxi
e-mail: an6428060@163.com